

Modelling pattern formation in soft flowing crystals

Andrea Montessori^{*1}, Marco Lauricella¹, Adriano Tiribocchi², and Sauro Succi^{2,1}

¹Istituto per le Applicazioni del Calcolo CNR, via dei Taurini 19, Rome, Italy

²Center for Life Nano Science@La Sapienza, Istituto Italiano di Tecnologia, 00161 Roma, Italy

June 23, 2020

Abstract

We present a mesoscale representation of near-contact interactions between colliding droplets which permits to reach up to the scale of full microfluidic devices, where such droplets are produced. The method is demonstrated for the case of colliding droplets and the formation of soft flowing crystals in flow-focussing microfluidic devices. This model may open up the possibility of multiscale simulation of microfluidic devices for the production of new droplet/bubble-based mesoscale porous materials.

1 Introduction

In the recent years, major advances in material science, fuelled by fundamental progress in condensed matter physics, have lead to important technological developments in many fields of science and engineering.

In particular, condensed matter physics has made substantial strides in the field of soft matter, namely the study of complex states of matter, typically composed of polymers, colloids, surfactants, liquid crystals, and other mesoscopic constituents, whose behaviour is dictated by energies at the thermal scale, i.e. “ kT ” physics.

Many soft materials exhibit physical and rheological properties which cannot be inferred directly from those of their constitutive elements [1, 2, 3, 4]. For instance, foams, binary mixtures of gas and liquid, display mechanical properties which cannot be traced back to either of the two [5, 6].

In this respect, progresses in microfluidic technologies have lead to a precise control over the production of bubbles and droplets in micro-channels, which can represent the fundamental constituents for the production of novel soft mesoscale materials [7, 8, 9, 10].

This has stimulated an outburst of experimental and theoretical activity alike, including computational methods, aiming at shedding light into the basic mechanisms controlling the behaviour of soft matter systems [11, 12, 13].

In particular, a wide body of theoretical and experimental work has elucidated the complex nature of the interactions occurring within intervening liquid films (i.e. near-contact interactions) [14, 15, 16, 17, 18, 19, 20, 21]. This laid down the foundations for describing a broad variety of complex systems, ranging from colloids, foams and emulsions, to flowing collections of droplets and bubbles characterized by highly ordered and uniform crystal-like structures, known as *soft flowing crystals* [22, 23].

Computational methods often permit to investigate parameter regions not accessible to experiments, and to explore non-perturbative regimes out of reach to analytical methods. However, the direct introduction of the near-contact forces is computationally prohibitive, as it requires to simultaneously solve almost six spatial decades: from millimeters, i.e. the typical size of microfluidic devices, all the way down to nanometers, namely the relevant spatial scale of contact forces [21].

Alternatively, a “softer” path can be taken. This does not require the direct introduction of nanoscale forces at the interface level, but relies on suitable coarse-grained models incorporating effective forces and potentials designed in such a way to retain the essential physics of soft interactions. While inherently approximate in nature, the latter alternative is very appealing, as it offers dramatic computational savings.

The success of such strategy is strictly dependent on the degree of universality of the underlying physics. Universality means dependence on suitable dimensionless groups rather than on the specific details of competing forces and interactions [24].

In this paper we show that a multicomponent lattice Boltzmann (LB) model [25, 26, 27, 21, 28], augmented with a suitable forcing term aimed at representing the effects of the near-contact forces operating at the fluid interface level [29, 30, 31], is capable of reproducing the droplets self-assembly and, for the first time, the morphology and self-tuning of the soft crystal patterns (from Hex-two to Hex-one structure) observed in microfluidic channels, in good agreement with previous experimental works [23, 32].

^{*}Electronic address: and.montessori@gmail.com; Corresponding author

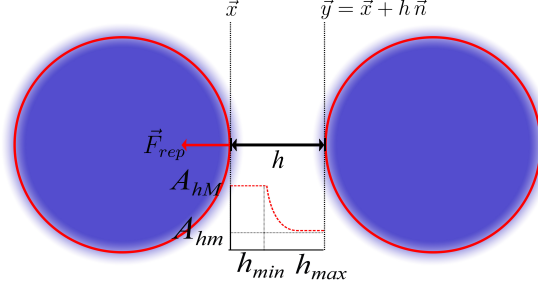


Figure 1: Near contact forces representation. Mesoscale modelling of near contact interactions between two immiscible fluid droplets. \vec{F}_{rep} represents the repulsive force and \vec{n} is the unit vector perpendicular to the fluid interface. The vectors \vec{x} and \vec{y} indicate the positions, placed a distance h , taken within the fluid interface and the dotted line tracks its outermost frontier. A_{hM} and A_{hm} are, respectively, the maximum and minimum value of the repulsive parameter.

2 Method

In this section, we provide a brief account of the numerical model, an extended color-gradient approach with repulsive near contact interactions, previously introduced in Ref. [27]. In the color gradient LB for multicomponent flows, two sets of distribution functions track the evolution of the two fluid components, according to the usual streaming-collision algorithm (see [33, 34]):

$$f_i^k(\vec{x} + \vec{c}_i \Delta t, t + \Delta t) = f_i^k(\vec{x}, t) + \Omega_i^k[f_i^k(\vec{x}, t)] + S_i(\vec{x}, t), \quad (1)$$

where f_i^k is the discrete distribution function, representing the probability of finding a particle of the k -th component at position \vec{x} , time t with discrete velocity \vec{c}_i , and S_i is a source term coding for the effect of external forces (such as gravity, near-contact interactions, etc). For further details about the LB equation see [33, 34]. The lattice time step is taken equal to 1, and the index i runs over the discrete lattice directions $i = 1, \dots, b$, where $b = 27$ for a three dimensional twenty-seven speed lattice (D3Q27). The density ρ^k of the k -th component and the total momentum of the mixture $\rho \vec{u} = \sum_k \rho^k \vec{u}^k$ are given by the zeroth and the first order moment of the distribution functions $\rho^k(\vec{x}, t) = \sum_i f_i^k(\vec{x}, t)$ and $\rho \vec{u} = \sum_i \sum_k f_i^k(\vec{x}, t) \vec{c}_i$. The collision operator splits into three components [35, 36, 37]:

$$\Omega_i^k = (\Omega_i^k)^{(3)} \left[(\Omega_i^k)^{(1)} + (\Omega_i^k)^{(2)} \right]. \quad (2)$$

In the above, $(\Omega_i^k)^{(1)}$, stands for the standard collisional relaxation [33], $(\Omega_i^k)^{(2)}$ is the perturbation step [35], which contributes to the buildup of the interfacial tension. Finally, $(\Omega_i^k)^{(3)}$ is the recoloring step [35, 38], which promotes the segregation between the two species, so as to minimise their mutual diffusion.

By performing a Chapman-Enskog expansion, it can be shown that the hydrodynamic limit of Eq.1 converges to a set of equations for the conservation of mass and linear momentum, with a capillary stress tensor of the form:

$$\Sigma = -\tau \sum_i \sum_k (\Omega_i^k)^{(2)} \vec{c}_i \vec{c}_i = \frac{\sigma}{2|\nabla \rho|} (|\nabla \rho|^2 \mathbf{I} - \nabla \rho \otimes \nabla \rho) \quad (3)$$

being τ the collision relaxation time, controlling the kinematic viscosity via the relation $\nu = c_s^2(\tau - 1/2)$ ($c_s = 1/\sqrt{3}$ the sound speed of the model), σ is the surface tension [33, 34] and \otimes denotes a dyadic tensor product.

The stress-jump condition across a fluid interface is augmented with a repulsive term aimed at providing a mesoscale representation of all the repulsive near-contact forces (i.e., Van der Waals, electrostatic, steric and hydration repulsion) acting on much smaller scales ($\sim O(1 \text{ nm})$) than those resolved on the lattice (typically well above hundreds of nanometers).

It takes the following form:

$$\mathbf{T}^1 \cdot \vec{n} - \mathbf{T}^2 \cdot \vec{n} = -\nabla(\sigma \mathbf{I} - \sigma(\vec{n} \otimes \vec{n})) - \pi \vec{n} \quad (4)$$

where $\pi[h(\vec{x})]$ is responsible for the repulsion between neighboring fluid interfaces, $h(\vec{x})$ being the distance along the normal \vec{n} , between locations \vec{x} and $\vec{y} = \vec{x} + h\vec{n}$ at the two interfaces, respectively (see Fig. 1).

The above expression can be recast in the following form [39]:

$$\mathbf{T}^1 \cdot \vec{n} - \mathbf{T}^2 \cdot \vec{n} = \sigma(\nabla \cdot \vec{n})\vec{n} - \nabla_t \sigma - \pi \vec{n} \quad (5)$$

in which ∇_t identifies the gradient tangent to the interface.

By neglecting any variation of the surface tension along the interface, we can approximate $\mathbf{T} = -p\mathbf{I}$ [40] and the above equation takes the following form:

$$(-p_1\mathbf{I}) \cdot \vec{n} - (-p_2\mathbf{I}) \cdot \vec{n} = \sigma(\nabla \cdot \vec{n})\vec{n} - \pi \vec{n} \quad (6)$$

By projecting the equation along the normal to the surface, we obtain the *extended* Young-Laplace equation [19, 41]:

$$(p_2 - p_1) = \sigma(\nabla \cdot \vec{n}) - \pi \quad (7)$$

The additional term can be readily included within the LB framework, by adding a forcing term acting only on the fluid interfaces in near contact, namely:

$$\vec{F}_{rep} = \nabla \pi := -A_h[h(\vec{x})]\vec{n}\delta_I \quad (8)$$

In the above, $A_h[h(\vec{x})]$ is the parameter controlling the strength (force per unit volume) of the near contact interactions, and is set equal to a constant A_{hM} if $h < h_{min}$, whereas it decreases as h^{-3} if $h > h_{min}$. The term h_{min} sets the threshold below which the repulsive force is effective. In our simulations we keep h_{min} equal to four lattice sites, and $A_{hM} = 0.05$. In addition, $h(\vec{x})$ is the distance between the interfaces, \vec{n} is a unit vector normal to the interface and $\delta_I \propto \nabla \phi$ is a function, proportional to the phase field $\phi = \frac{\rho^1 - \rho^2}{\rho^1 + \rho^2}$, that localizes the force at the interface.

The further repulsive force (added to the right hand side of Eq. 1) naturally leads to the following (extended) conservation law for the momentum equation:

$$\frac{\partial \rho \vec{u}}{\partial t} + \nabla \cdot \rho \vec{u} \vec{u} = -\nabla p + \nabla \cdot [\rho \nu (\nabla \vec{u} + \nabla \vec{u}^T)] + \nabla \cdot (\Sigma + \pi \mathbf{I}) \quad (9)$$

This is the Navier-Stokes equation for a multicomponent system, augmented with a surface-localized repulsive term, expressed through the gradient of the potential function π .

3 Results

In the following, we demonstrate the proposed scheme for two relevant applications, the collision of immiscible liquid droplets and the formation of flowing crystals in microfluidic devices.

3.1 Colliding droplets

We first show the capability of the extended LB model to accurately reproduce the correct dynamics of off-axis collisions between two immiscible droplets [42]. The characteristic non-dimensional parameters, governing the collision outcome are the Weber and the Reynolds numbers, defined as $We = \rho U_{rel}^2 D / \sigma$ and $Re = U_{rel} D / \nu$, respectively. In the above, U_{rel} the relative impact velocity, D the droplet diameter, σ the surface tension coefficient and ν the kinematic viscosity, as well as the impact number $b = \chi / D$, namely, the distance between the collision trajectories in units of the droplet diameter.

In this simulation the values of the physical and geometrical parameters are: domain size $121 \times 101 \times 121$ ($nx \times ny \times nz$), droplets diameter $D = 30$, relative speed between the impacting droplets $U_{rel} = 0.06$, surface tension $\sigma = 0.01$, magnitude of the repulsive force $A_h = 0.01$, kinematic viscosity $\nu = 0.0167$, Weber number $We = 10$, Reynolds number $Re = 108$ and impact number $b = 0.33$.

In figure 2(a) we report the collision sequence between the droplets and compare the numerical results with the experimental data reported in [42]. The experiments were performed using liquid droplets with diameters ranging between $700 - 800 \mu m$ and impact velocities in the range of $1 - 3 m/s$.

As shown in panel (a) of figure 2, the two droplets undergo a kiss and tumble collision, in close agreement with the experiment.

It is worth noting that the additional repulsive force proves instrumental to reproduce this collision outcome. Indeed, the coalescence between the droplets is frustrated by the effect of the near-contact repulsive forces, which prevent the rupture of the intervening thin film between the impacting droplets.

We then inspected the evolution of the thin liquid film during the collision process. As reported in fig. 2b (left), the fluid between the two approaching droplets first flows outwards, and then recirculates within the intervening film, producing a decrease in the fluid pressure (fig. 2b, right) that temporarily stabilizes the film and prevents the droplets' coalescence. After the collision, droplets are scattered far apart and the film gradually disappears.

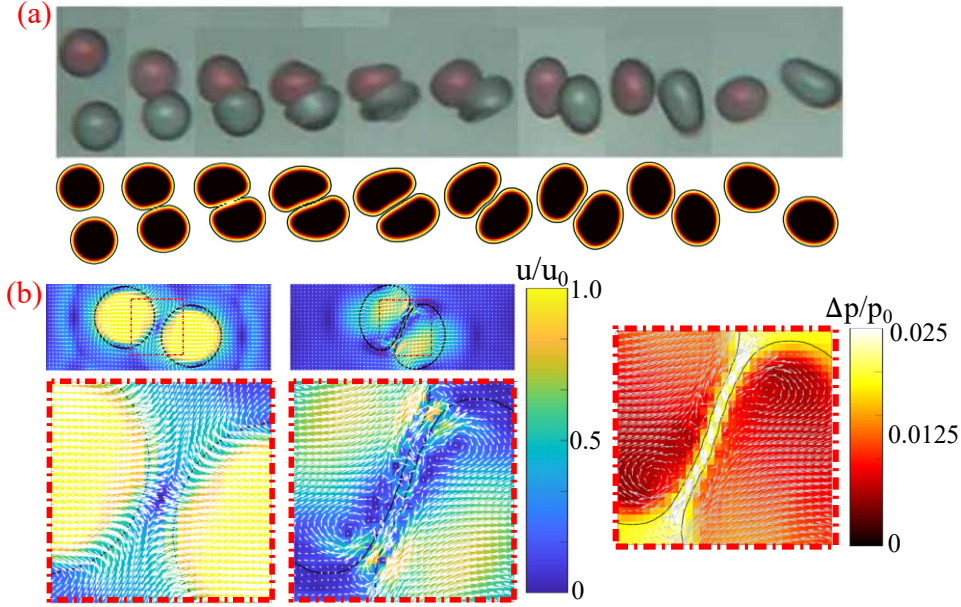


Figure 2: (a) Collision sequence with $b = 0.33$ and $We = 10$. The upper row shows the experiments of Ref. [42], the lower row shows the simulation results. (b) Left. Sequence of the flow field during the impact between the two droplets (mid-plane slice). During the first stage of the collision the dispersed phase flows outwards, allowing the two droplets to approach. Afterwards, when the droplets come in close contact, the fluid within the thin film begins to recirculate, thereby preventing film rupture, hence the coalescence between the droplets. (b) Right. Map of the local pressure deviation $\Delta p/p_0 = (p_0 - p)/p_0$, where p_0 is the bulk pressure of the surrounding fluid and p is the local pressure. As shown in the figure, the outer fluid is driven inwards and consequently stabilizes the film.

The observed phenomenon resembles the so-called *Marangoni flow* in liquid films, namely a fluid recirculation occurring in liquid thin films in the presence of shear and temperature gradients, which has been observed to prevent the coalescence between bodies of liquids [43].

3.2 Crystal patterns in microchannels

We then performed three-dimensional simulations of a oil/water emulsion in a microfluidic flow-focusing device [44, 45]. The micro-device is made of three inlet channels ($H = 200\mu m$), supplying the dispersed and the continuous phase, an orifice placed downstream the three coaxial inlet streams ($h = 100\mu m$) plus an outlet channel of height $H_c = 400\mu m$ and length $1.9 \times 10^3\mu m$. The width of the focuser (the dimension perpendicular to the flow direction) is $W = 100\mu m$. In our simulations we consider a device in which the thickness of the inlet and of the outlet channels is $L_x = 20$ (perpendicular to the plane), while their height is $L_z = 80$. Moreover, the length of the outlet channel is $L_y = 420$, that of the inlet one is $L_y = 40$, and the orifice is cubic shaped with dimensions $20 \times 20 \times 20$. Finally, we use no-slip conditions on both walls and, to achieve hydrophobicity, we set the contact angle with the dispersed phase at $\simeq 130^\circ$.

The mechanism of droplet formation follows from the periodic pinch-off of the dispersed jet by the continuous stream and the pinch-off mechanism takes place in the small orifice.

Such microfluidic geometry is widely employed for the production of foams and emulsions, as it offers an accurate control over the monodispersity and the droplet size [46, 47, 48]. The high degree of flow reproducibility is due to the dominance of the viscous forces over inertia, which smoothens the flow and tames hydrodynamic instabilities. The periodic pinch-off process permits to produce droplets with standard deviations in size as little as the 0.1% [49, 50, 44].

Here, we show that the proposed approach is able to reproduce different crystal patterns in the outlet channel of the device.

By taking an interfacial tension of an oil-water mixture ($\sim 50mN/m$), the dynamic viscosity of the water (dispersed phase) $\mu \sim 10^{-3}Pa \cdot s$ and an inlet velocity of the dispersed phase $\sim 0.1m/s$, we obtain a Weber number $We = 0.04$ and a capillary number $Ca = 0.0017$. The droplet production can be controlled by tuning the dispersed to continuous flow rate ratio and, when the density of droplets is sufficiently high, an emulsion is formed within the exit micro-channel. As reported in figure 3, different crystalline structures

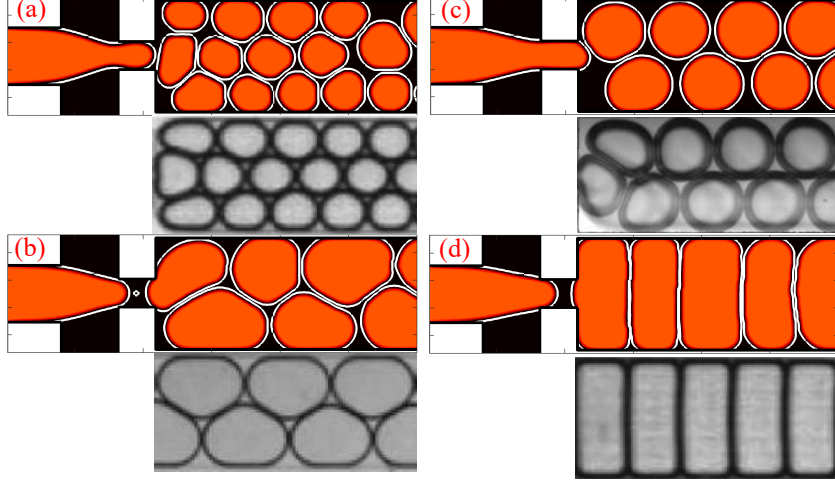


Figure 3: (a -b) Emulsion structures in microchannels. The different patterns are obtained by tuning the dispersed-to-continuous inlet flow ratios from $\phi = u_d/2u_c = 1 \div 3.6$. Simulations are compared against the experiments of Marmottant et al. [23]. (a) Hex-Three, (b) Wet Hex-Two, (c) Dry Hex-Two, (d) Hex-One.

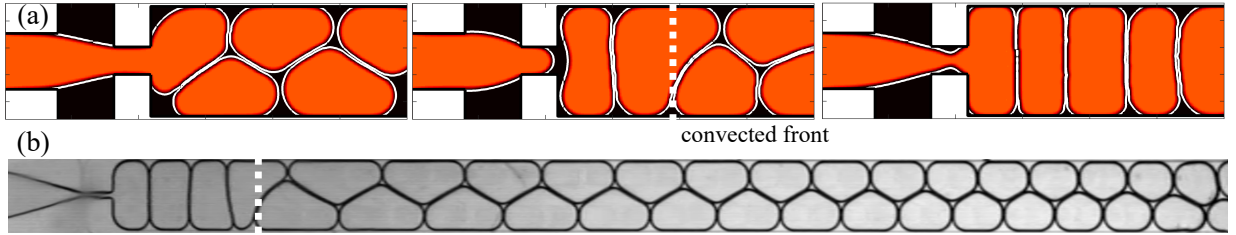


Figure 4: (a -b) Spontaneous dynamic rearrangement of the emulsion pattern within the outlet micro-channel ((a) numerical simulations, (b) experiments). The vertical bars indicate the rearrangement fronts. Lower panel, experimental snapshot taken from [23]

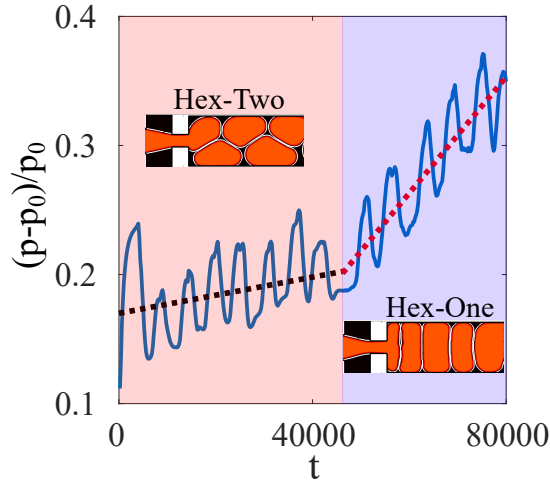


Figure 5: Non dimensional pressure variation (p_0 is a reference bulk pressure) within the inlet main channel of the dispersed phase as a function of time. The dotted lines are linear fits to the data. The transition from an Hex-Two to an Hex-One crystal is clearly indicated by a sudden jump in the slopes of the linear fits.

appear when lowering the inlet dispersed fluid discharge for a constant inlet continuous phase flow rate: the droplets arrangement within the microchannel transits from a Hex-three structure, typical of flowing emulsions in microchannels, to wet and dry Hex-two structures, with the droplets self-arranging in a ordered two files configuration, up to the "bamboo" structure typical of Hex-one-like emulsions. Remarkably, the numerical model employed, is able to seamlessly and accurately capture all these regimes, as evidenced in figure 3, in which the pattern obtained by means of numerical simulations are compared with those reported in [32, 23].

Between these homogeneous crystal patterns, we also observed a self-regulated transition flow, in agreement with [23], as reported in figure 4. This intermediate regime is associated with a rich dynamic behaviour, resulting in structures that vary over space and time within the channel and controlled by the speed of the foam.

In particular, we observe a spontaneous transition regime in which the Hex-two and the Hex-one structures simultaneously coexist. This regime is characterized by the presence of a rearrangement front travelling within the outlet channel along the flow direction with a speed smaller than that of the foam (see [32]). As observed in [23], this meta-stable regime strikingly resembles a thermodynamic first order transition.

Moreover, we inspected the pressure field within the inlet channel of the dispersed component, noting that the transition between the two crystal patterns is signaled by a rapid increase of the pressure of the dispersed phase, which is a feedback effect of the partial clogging of the outlet channel caused by the droplets arranged in a two files Hex-two crystal. The pressure undulations are arguably due to the periodic pinch-off of the droplet within the orifice and its subsequent injection in the outlet channel. This complex flow is a genuine example of dynamic self-organization in microfluidic channels which prospects new chances for the generation of highly controlled emulsions.

In particular, this intermediate regime offers a route to the production of droplets samples with a controlled polydispersity.

4 Conclusions and future outlook

Summarising, we have presented a new lattice Boltzmann method for multicomponent fluids, augmented with near-contact repulsion between approaching droplets, due to the presence of surfactant molecules.

The near-contact interactions are represented by coarse-grained effective forces which, besides preventing droplet coalescence, prove capable of predicting non-trivial large-scale features of the flow, such as the formation of regular configurations of flowing droplets, known as soft flowing crystals.

The success of the method crucially hinges on the universality of the underlying physics; in other words, the key requirement on near-contact interactions is to prevent droplet coalescence, and once this feature is secured, the highly non-trivial dynamics which develops at larger space and time scales goes under control of other mechanisms, such as capillarity and hydrodynamic interactions, which are also taken in charge by the mesoscale lattice Boltzmann method.

Whilst based on a dramatic simplification of the underlying physics at the molecular level, the results obtained in this paper suggest that, at least at the spatial scale at hand, a coarse grained description is appropriate to describe the mesoscale evolution of an interacting multidroplet system.

The present work is expected to benefit the multiscale simulation of microfluidic devices for the production of new droplet/bubble-based mesoscale porous materials.

5 Acknowledgments

A. M., M. L., A. T. and S. S. acknowledge funding from the European Research Council under the European Union's Horizon 2020 Framework Programme (No. FP/2014-2020) ERC Grant Agreement No.739964 (COPMAT).

References

- [1] A. Tiribocchi, F. Bonaccorso, M. Lauricella, S. Melchionna, A. Montessori, S. Succi, Curvature dynamics and long-range effects on fluid-fluid interfaces with colloids, *Soft Matter* 15 (2019) 2848–2862. doi:10.1039/C8SM02396D.
- [2] Y. Gai, A. Bick, S. K. Y. Tang, Timescale and spatial distribution of local plastic events in a two-dimensional microfluidic crystal, *Phys. Rev. Fluids* 4 (2019) 014201. doi:10.1103/PhysRevFluids.4.014201. URL <https://link.aps.org/doi/10.1103/PhysRevFluids.4.014201>
- [3] P. Sollich, F. Lequeux, P. Hébraud, M. E. Cates, Rheology of soft glassy materials, *Physical review letters* 78 (10) (1997) 2020.
- [4] J. Goyon, A. Colin, G. Ovarlez, A. Ajdari, L. Bocquet, Spatial cooperativity in soft glassy flows, *Nature* 454 (7200) (2008) 84.
- [5] B. Dollet, A. Scagliarini, M. Sbragaglia, Two-dimensional plastic flow of foams and emulsions in a channel: experiments and lattice boltzmann simulations, *Journal of Fluid Mechanics* 766 (2015) 556–589.
- [6] Y. Gai, C. M. Leong, W. Cai, S. K. Tang, Spatiotemporal periodicity of dislocation dynamics in a two-dimensional microfluidic crystal flowing in a tapered channel, *Proceedings of the National Academy of Sciences* 113 (43) (2016) 12082–12087.
- [7] W. Li, L. Zhang, X. Ge, B. Xu, W. Zhang, L. Qu, C.-H. Choi, J. Xu, A. Zhang, H. Lee, D. A. Weitz, Microfluidic fabrication of microparticles for biomedical applications, *Chem. Soc. Rev.* 47 (2018) 5646–5683.
- [8] E. Stolovicki, R. Ziblat, D. A. Weitz, Throughput enhancement of parallel step emulsifier devices by shear-free and efficient nozzle clearance, *Lab on a Chip* 18 (1) (2018) 132–138.
- [9] A. Montessori, M. Lauricella, S. Succi, E. Stolovicki, D. Weitz, Elucidating the mechanism of step emulsification, *Phys. Rev. Fluids* 3 (2018) 072202. doi:10.1103/PhysRevFluids.3.072202. URL <https://link.aps.org/doi/10.1103/PhysRevFluids.3.072202>
- [10] A. Montessori, M. Lauricella, E. Stolovicki, D. A. Weitz, S. Succi, Jetting to dripping transition: Critical aspect ratio in step emulsifiers, *Physics of Fluids* 31 (2) (2019) 021703.
- [11] T. Murtola, A. Bunker, I. Vattulainen, M. Deserno, M. Karttunen, Multiscale modeling of emergent materials: biological and soft matter, *Phys. Chem. Chem. Phys.* 11 (2009) 1869–1892. doi:10.1039/B818051B.
- [12] G. Falcucci, S. Ubertini, C. Biscarini, S. Di Francesco, D. Chiappini, S. Palpacelli, A. De Maio, S. Succi, Lattice boltzmann methods for multiphase flow simulations across scales, *Communications in Computational Physics* 9 (2) (2011) 269–296.
- [13] M. P. Allen, D. J. Tildesley, *Computer simulation of liquids*, Oxford university press, 2017.
- [14] B. V. Derjaguin, On the repulsive forces between charged colloid particles and on the theory of slow coagulation and stability of lyophobic sols, *Trans. Faraday Soc.* 36 (1940) 730.
- [15] B. V. Derjaguin, L. D. Landau, Theory of the stability of strongly charged lyophobic sols and of the adhesion of strongly charged particles in solutions of electrolytes, *Acta Physicochimica U.R.S.S.* 14 (1941) 633–662.
- [16] E. J. W. Verwey, J. T. H. G. a. Overbeek, *Theory of the stability of lyophobic colloids*, Amsterdam: Elsevier, 1948.

- [17] G. B. Webber, S. A. Edwards, G. W. Stevens, F. Grieser, R. R. Dagastine, D. Y. C. Chan, Measurements of dynamic forces between drops with the afm: novel considerations in comparisons between experiment and theory, *Soft Matter* 4 (2008) 1270.
- [18] R. R. Dagastine, R. Manica, S. L. Carnie, D. Y. C. Chan, S. G. W., F. Grieser, Dynamic forces between two deformable oil droplets in water, *Science* 313 (2006) 210–213.
- [19] D. Y. Chan, E. Klaseboer, R. Manica, Film drainage and coalescence between deformable drops and bubbles, *Soft Matter* 7 (6) (2011) 2235–2264.
- [20] W. Wang, K. Li, M. Ma, H. Jin, P. Angeli, J. Gong, Review and perspectives of afm application on the study of deformable drop/bubble interactions, *Adv. Colloid Interface Sci.* 225 (2015) 88–97.
- [21] A. Montessori, M. Lauricella, S. Succi, Mesoscale modelling of soft flowing crystals, *Phil. Trans. Roy. Soc., Ser. A* 377 (2019) 20180149.
- [22] P. Garstecki, G. M. Whitesides, Flowing crystals: nonequilibrium structure of foam, *Phys. Rev. Lett.* 97 (2006) 024503.
- [23] J.-P. Raven, P. Marmottant, Microfluidic crystals: Dynamic interplay between rearrangement waves and flow, *Phys. Rev. Lett.* 102 (2009) 084501. doi:10.1103/PhysRevLett.102.084501.
URL <https://link.aps.org/doi/10.1103/PhysRevLett.102.084501>
- [24] S. Succi, Lattice boltzmann 2038, *EPL (Europhysics Letters)* 109 (5) (2015) 50001.
- [25] F. Higuera, S. Succi, R. Benzi, Lattice gas dynamics with enhanced collisions, *EPL (Europhysics Letters)* 9 (4) (1989) 345.
- [26] A. Montessori, P. Prestininzi, M. La Rocca, S. Succi, Lattice boltzmann approach for complex nonequilibrium flows, *Phys. Rev. E* 92 (4) (2015) 043308.
- [27] A. Montessori, M. Lauricella, N. Tirelli, S. Succi, Mesoscale modelling of near-contact interactions for complex flowing interfaces, *Journal of Fluid Mechanics* 872 (2019) 327–347.
- [28] A. Montessori, M. Lauricella, M. La Rocca, S. Succi, E. Stolovicki, R. Ziblat, D. Weitz, Regularized lattice boltzmann multicomponent models for low capillary and reynolds microfluidics flows, *Computers & Fluids* 167 (2018) 33–39.
- [29] R. Benzi, S. Chibbaro, S. Succi, Mesoscopic lattice boltzmann modeling of flowing soft systems, *Physical review letters* 102 (2) (2009) 026002.
- [30] M. Sbragaglia, R. Benzi, M. Bernaschi, S. Succi, The emergence of supramolecular forces from lattice kinetic models of non-ideal fluids: applications to the rheology of soft glassy materials, *Soft Matter* 8 (41) (2012) 10773–10782.
- [31] L. Fei, A. Scagliarini, A. Montessori, M. Lauricella, S. Succi, K. H. Luo, Mesoscopic model for soft flowing systems with tunable viscosity ratio, *Physical Review Fluids* 3 (10) (2018) 104304.
- [32] P. Marmottant, J. P. Raven, Microfluidics with foams, *Soft Matter* 5 (2009) 3385–3388.
- [33] S. Succi, *The Lattice Boltzmann Equation: For Complex States of Flowing Matter*, Oxford University Press, 2018.
- [34] T. Krüger, H. Kusumaatmaja, A. Kuzmin, O. Shardt, G. Silva, E. M. Viggen, *The lattice boltzmann method*, Springer International Publishing 10 (2017) 978–3.
- [35] A. K. Gunstensen, D. H. Rothman, S. Zaleski, G. Zanetti, Lattice boltzmann model of immiscible fluids, *Physical Review A* 43 (8) (1991) 4320.
- [36] S. Leclaire, M. Reggio, J.-Y. Trépanier, Numerical evaluation of two recoloring operators for an immiscible two-phase flow lattice boltzmann model, *Applied Mathematical Modelling* 36 (5) (2012) 2237–2252.
- [37] S. Leclaire, A. Parmigiani, O. Malaspinas, B. Chopard, J. Latt, Generalized three-dimensional lattice boltzmann color-gradient method for immiscible two-phase pore-scale imbibition and drainage in porous media, *Physical Review E* 95 (3) (2017) 033306.
- [38] M. Latva-Kokko, D. H. Rothman, Diffusion properties of gradient-based lattice boltzmann models of immiscible fluids, *Physical Review E* 71 (5) (2005) 056702.

- [39] J. Li, Macroscopic model for head-on binary droplet collisions in a gaseous medium, *Physical review letters* 117 (21) (2016) 214502.
- [40] J. Brackbill, D. B. Kothe, C. Zemach, A continuum method for modeling surface tension, *Journal of computational physics* 100 (2) (1992) 335–354.
- [41] M. B. Williams, S. H. Davis, Nonlinear theory of film rupture, *Journal of Colloid and Interface Science* 90 (1) (1982) 220–228.
- [42] R.-H. Chen, C.-T. Chen, Collision between immiscible drops with large surface tension difference: diesel oil and water, *Experiments in Fluids* 41 (3) (2006) 453–461. doi:10.1007/s00348-006-0173-2. URL <https://doi.org/10.1007/s00348-006-0173-2>
- [43] P. Dell'Aversana, J. R. Banavar, J. Koplik, Suppression of coalescence by shear and temperature gradients, *Physics of Fluids* 8 (1) (1996) 15–28.
- [44] D. R. Link, S. L. Anna, D. A. Weitz, H. A. Stone, Geometrically mediated breakup of drops in microfluidic devices, *Phys. Rev. Lett.* 92 (2004) 054503. doi:10.1103/PhysRevLett.92.054503. URL <https://link.aps.org/doi/10.1103/PhysRevLett.92.054503>
- [45] P. Garstecki, I. Gitlin, W. DiLuzio, G. M. Whitesides, E. Kumacheva, H. A. Stone, Formation of monodisperse bubbles in a microfluidic flow-focusing device, *Applied Physics Letters* 85 (13) (2004) 2649–2651.
- [46] G. M. Whitesides, The origins and the future of microfluidics, *Nature* 442 (7101) (2006) 368.
- [47] E. K. Sackmann, A. L. Fulton, D. J. Beebe, The present and future role of microfluidics in biomedical research, *Nature* 507 (7491) (2014) 181.
- [48] F. Cruz-Mazo, M. A. Herrada, A. M. Ganan-Calvo, J. M. Montanero, Global stability of axisymmetric flow focusing, *Journal of Fluid Mechanics* 832 (2017) 329–344. doi:10.1017/jfm.2017.684.
- [49] P. Marmottant, J.-P. Raven, Microfluidics with foams, *Soft Matter* 5 (18) (2009) 3385–3388.
- [50] A. M. Ganan-Calvo, J. M. Gordillo, Perfectly monodisperse microbubbling by capillary flow focusing, *Physical review letters* 87 (27) (2001) 274501.